Journal of the European Ceramic Society 21 (2001) 603–610

www.elsevier.com/locate/jeurceramsoc

Origin of the strength change of silicon nitride ceramics with the alteration of spray drying conditions

Tadashi Hotta [a], Kenji Nakahira [a], Makio Naito [a,*], Nobuhiro Shinohara [b], Masataro Okumiya [b], Keizo Uematsu [c]

[a] *Japan Fine Ceramics Center, 2-4-1, Mutsuno, Atsuta-ku, Nagoya 456-8587, Japan*
[b] *Research Center, Asahi Glass Co., Ltd., Hazawa-cho, Kanagawa-ku, Yokohama, 221-8755, Japan*
[c] *Department of Chemistry, Nagaoka University of Technology, 1603-1, Kamitomioka-cho, Nagaoka 940-2188, Japan*

Received 15 January 2000; received in revised form 23 July 2000; accepted 31 July 2000

Abstract

The effect of changing the spray drying conditions on the microstructure of green bodies and on the strength variation of sintered bodies was examined for silicon nitride ceramics. Novel characterization techniques were applied to observe the internal structure of granules, green bodies and the resultant ceramics. As a result, the difference of the fracture strength of sintered bodies made from the granular compaction route could be explained quantitatively by the difference of the pore size distribution in the sintered bodies. Those potential flaws were introduced by the incomplete collapse of dimples in granules and of interstices between granules. Different characteristics of granules exerted a serious influence on the size and concentration of potential flaws in green compacts and on the resultant mechanical strength of sintered bodies after densification.

Keywords: Fracture origin; Granules; Mechanical properties; Si_3N_4; Spray drying

1. Introduction

It has been known that the manufacturing conditions exert a very significant influence on the unpredictable variation of the fracture strength of ceramic products. Each step in processing has the potential for introducing detrimental defects such as large grains, aggregates, or large pores.[1] For powder processing using granules, heterogeneities are often introduced in the green compacts during forming; they then either persist or develop to form defects that govern the strength of the ceramics during the subsequent densification and microstructure development.[2–7] It is thus crucial to identify the dominant flaw in a ceramic material in each processing step and to eliminate it by the proper modification of the processing conditions. The extremely low concentration of such defects, however, makes it difficult to detect them by conventional characterization tools, such as SEM and mercury porosimetry.

Considerable use has been made of the new characterization techniques developed by Uematsu et al.[8–12] for the identification of heterogeneities in granules, green and sintered bodies of alumina ceramics; the techniques have successfully revealed the influence of minor differences in processing conditions during spray-drying, forming and sintering on the development of fracture origins.[4–6] We found that large pores were especially active as dominant flaws for the undesirable variation of fracture strength in alumina ceramics made through the granular compaction route.

Even in silicon nitride ceramics, large pores resulting from heterogeneities in green compacts are known to become fracture origins responsible for the degradation of fracture strength.[2,3,13] However, the mechanism of the formation or the development of large pores in silicon nitride densified by liquid phase sintering is not well understood, although it is expected to be different from the mechanism in solid-state sintered alumina ceramics.

In this study, three kinds of granules were prepared from the same slurry of silicon nitride by changing the spray drying conditions; notably the inlet air temperature for spray-drying and the feed rate of slurry. Dense

* Corresponding author. Tel.: +81-52-871-3500; fax: +81-52-871-3599.
E-mail address: naito@jfcc.or.jp (M. Naito).

0955-2219/01/$ - see front matter
PII: S0955-2219(00)00243-0

Table 1
The raw materials and their amounts used for experiments

Material	Function	Manufacturer	Grade	Amount (g)
Silicon nitride	Powder	Ube	SN-E10	270
Alumina	Powder	Sumitomo Chemical Co., Ltd	AKP-30	15
Yttrium oxide	Powder	Daiichi Kigenso Kagaku Kogyo Co.,	NRN	15
Polyvinyl alcohol	Binder	Shinetsu Chemical Co., Ltd	PV-3	22.5
Polyethylene glycol	Plasticizer	Nippon Oil	#4000	4.7
Stearic acid emulsion	Lubricant	Chukyo Yushi Co., Ltd	Selosol 920	15

silicon nitride ceramics were obtained by the pressureless sintering of green bodies fabricated with these granules, and the properties of the sintered bodies, i.e. density, fracture strength, and fracture toughness, were determined. Transmission characterization methods were applied to identify the heterogeneities of the products after each processing step with a view to clarifying the formation mechanism of the large pore defects. The influence of the size and concentration of pore defects on the strength variation is also discussed.

2. Experimental procedure

The starting raw materials and the manufacturing process for the experiments are presented in Table 1 and Fig. 1, respectively. Commercially available silicon nitride, alumina and yttria powders were used as the starting materials. The average particle size of each powder measured by X-ray sedimentation is 0.44, 0.33, and 0.29 μm, respectively. The silicon nitride powder was mixed with alumina and yttria by ball-milling with distilled and deionized water for 24 h. The concentration of the powder mixtures was 65.9 mass%. Dispersant was not added because the pH of the slurry moved to the basic region (~9.5), at which silicon nitride could be deflocculated electrostatically, due to the reaction of silicon nitride and water during mixing. The slurry was passed through a sieve (32 μm) to remove large agglomerates or inclusions, then mixed again in a stirrer mixer with binder (polyvinyl alcohol), plasticizer (polyethylene glycol) and lubricant (stearic acid emulsion). The concentration of each additive was 0.9, 0.45, and 0.9 mass%, respectively. After mixing, the slurry was dried to form granules under the three different drying conditions A, B and C, as shown in Table 2, by using a spray dryer (TRS-5W, Sakamoto Giken Co., Ltd., Japan). The rotating speed of the rotary atomizer was adjusted to be 8000 rpm in all cases. All granules were sieved through a 150 μm screen for the removal of large agglomerates and foreign objects before the testing.

The consolidation behavior of the granules was analyzed by a compression tester, Aggrobot (Hosokawa Micron Corp., Osaka, Japan).[14] In this experiment, granules were poured into a cylinder with an inner diameter of 15 mm. The initial height of the granule beds was set at about 35 mm. A compressive stress was exerted uniaxially on the granule bed at a speed of 0.1 mm/s until it reached 11.1 MPa.

For sintering, granules were uniaxially pressed in a rectangular metal die (60×50 mm) at 19.6 MPa. After dewaxing by heat-treating at 530°C for 15 h in an electric furnace, the mold-pressed samples were CIPed at 294 MPa to form green compacts. The green bodies were embedded in boron nitride powders in a silicon nitride container and heated at 1700°C for 3 h for sintering

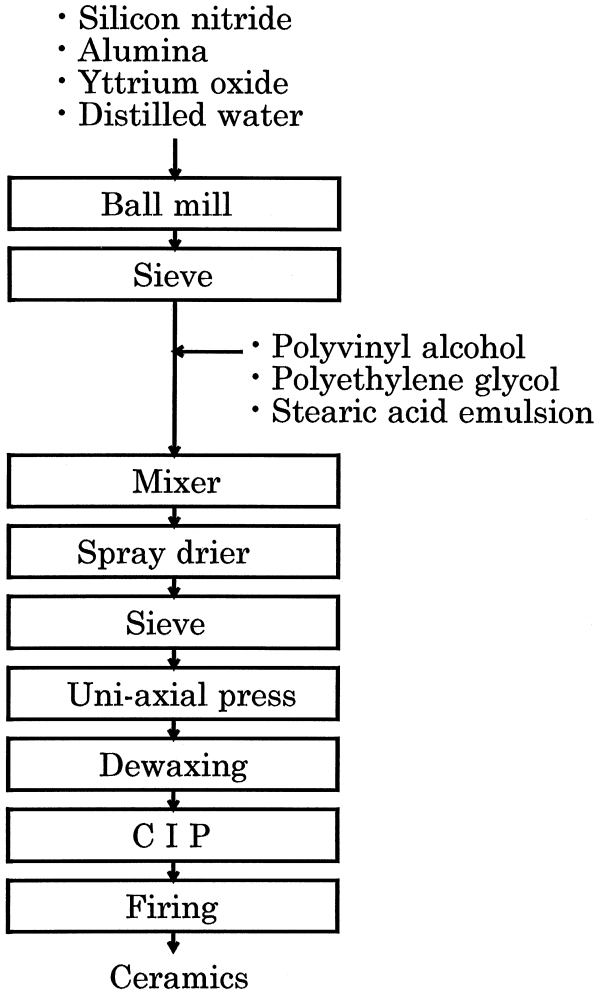

Fig. 1. Fabrication process of silicon nitride ceramics.

Table 2
Spray drying conditions

	A	B	C
Inlet air temperature (°C)	160	200	160
Feed slurry amount (g/min)	100	100	200

under 0.1 MPa nitrogen atmosphere. Densities of all sintered samples were measured by the Archimedes method with water.

The internal structures of the granules and green bodies were examined by direct observation techniques. For the structural observation of green bodies, the samples were thinned to a tenth of a millimeter thick with grinding paper. A few drops of an immersion liquid with a refractive index 2.05, which is almost same as that of alumina, was added to make them transparent and to observe the structure optically in the transmission mode.[2] For the structural observation of sintered bodies, samples were thinned to a thickness of less than about 50 μm to make them transparent and were subjected to the same optical microscope examination without adding immersion liquid.[19] The microstructure of sintered specimens was also examined by using SEM. Mercury porosimetry (Autopore II 9220, Micromeritics) was employed to determine the size and the size distribution of pore channels in the green compacts.

Fracture strength and fracture toughness were examined by using specimens with size 3×4×40mm cut from the sintered samples. The surfaces of the specimens were finished with a diamond grinding wheel of #800. The method specified by JIS R 1601 was applied to measure the strength in four point bending with outer and inner span lengths of 30 and 10 mm, respectively. The cross head speed was adjusted to 0.5 mm/min. Fracture toughness was also measured by applying the single-edged-precracked beam method specified by JIS R1607.

3. Results

Fig. 2 shows the size distribution data of spray dried granules made with the conditions A, B and C, in Table 2. In the following description, products made through each spray-drying condition are named A, B and C, respectively. All conditions produced wide size distributions ranging from 30 to 150 μm, although the curves were slightly different. Granules A and B show almost identical distribution curves with average diameters of 69 and 72 μm, respectively. Granules C have clearly larger size (89 μm).

Fig. 3 shows a typical example of the internal structure of granules taken with the transmission mode for granules B. Dimples are clearly visible in the majority of cases. Dimples were also found in granules A and C. The size of the dimples tended to become larger in proportion to the size of granules.

Fig. 4 shows the compression behavior of a granule bed for granules A, B and C, respectively. The compression of the granule bed occurs in two steps for all granules: the first one is characterized by a low slope and the second by a relatively steep curve. The gradients in the relatively steep curves were almost same in these three types of granules. It was, however, found that the low slope was different for each type of granule. The critical stress, p_c, determined by the intersection of the straight lines fitted to the low pressure and the high pressure legs was 0.75, 0.99, and 0.83 MPa for granules A, B, and C, respectively.

Fig. 5 shows the pore size distribution curves of CIPed green bodies determined by mercury porosimetry. All samples showed nearly the same characteristics for the pore size distribution. No clear evidence was noted for the retainment of large, intergranular pores by this conventional characterization tool.

Fig. 6 shows a photomicrograph taken in the transmission mode with the liquid immersion method for a green compact B. The shape of granules is clearly visible in the internal structure even after CIPing at a high compaction pressure. It should also be remarked that large voids were found in and between granules. Similar

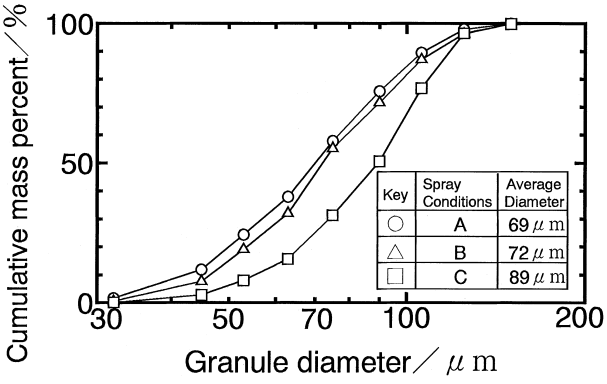

Fig. 2. Size distributions of granules.

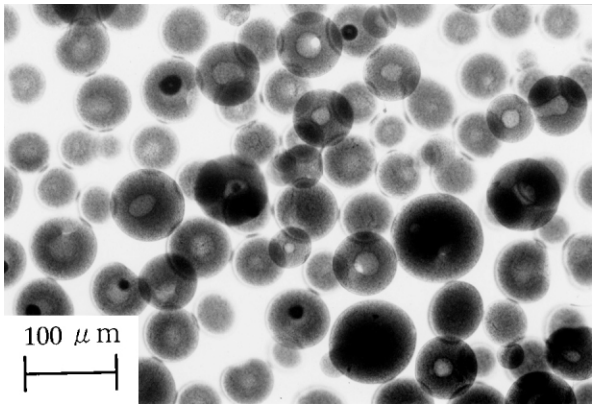

Fig. 3. Transmission optical micrograph of granules (B).

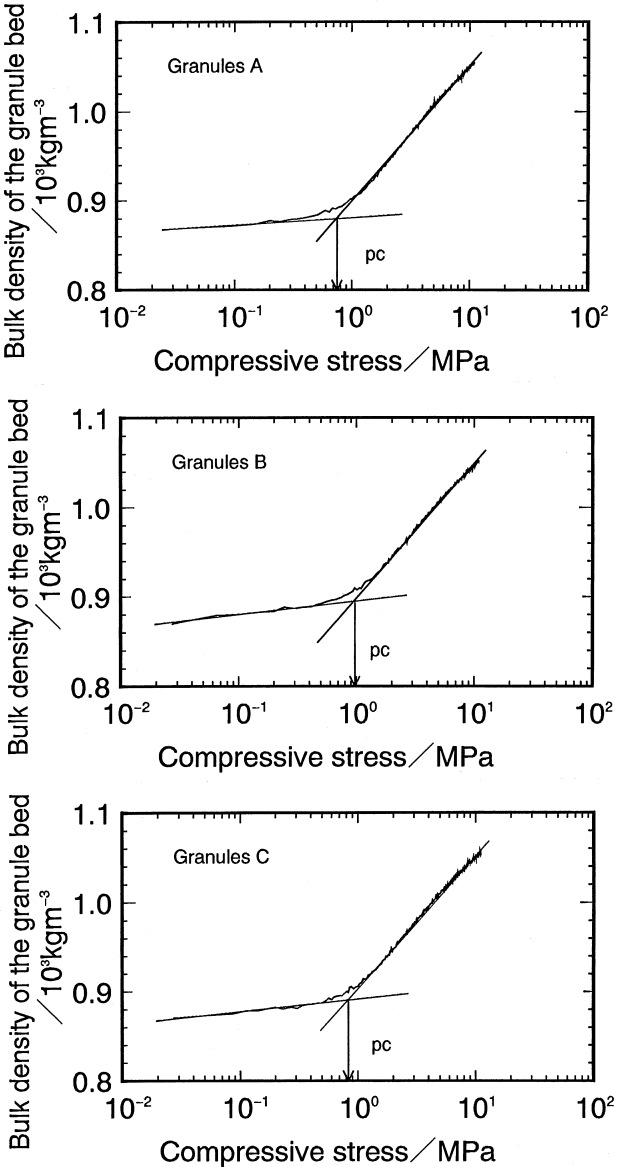

Fig. 4. The consolidation curves of granule compacts.

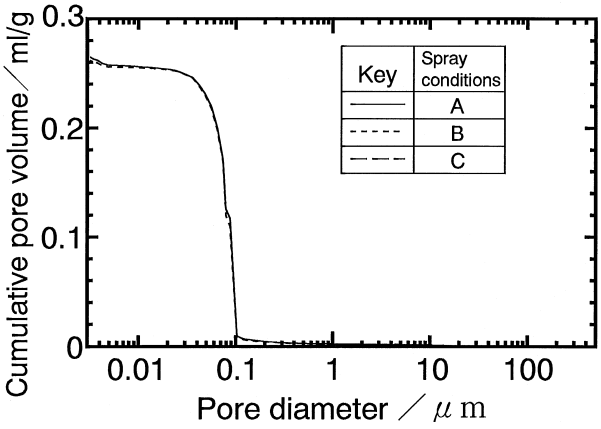

Fig. 5. Pore size distributions of green compacts.

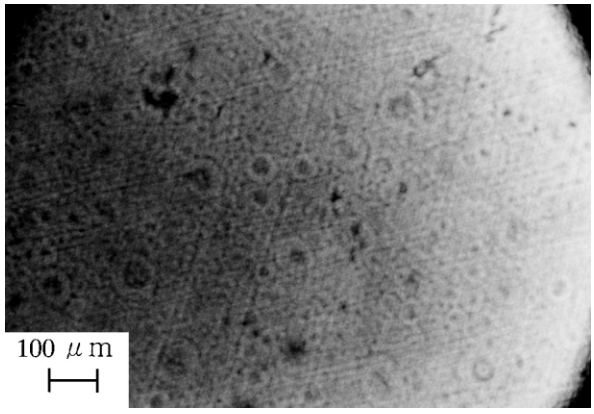

Fig. 6. Transmission optical micrograph of green compact (B).

Table 3
Density and fracture toughness of specimens

Specimens	Density (kg/m^3)	Fracture toughness ($MPa\ m^{1/2}$)
Made from granules A	3.21×10^3	5.0
Made from granules B	3.22×10^3	5.1
Made from granules C	3.21×10^3	5.0

structure was also observed in green compacts A and C. The results clearly show that the voids are preserved even in highly compacted green bodies, although the concentration of them must be low because they are not detected with mercury porosimetry.

Table 3 shows the density and fracture toughness of sintered specimens. As shown, these were almost the same for all samples. Relatively low fracture toughness in the present samples is probably due to the insufficient growth of elongated grains caused by the low temperature sintering at 1700°C.

Fig. 7 shows the Weibull distribution curves of the flexural strength for the sintered bodies. A clear difference was noted in the fracture strength depending on the type of granule. Average strength was the highest for sample C (766 MPa) and decreased in the order of sample A (722 MPa) and B (685 MPa), although the calculated Weibull moduli were high for all samples. The distribution curves showed nearly parallel lines, suggesting that the dominant defects for the fracture were of the same origin.

Fig. 8 shows a SEM micrograph taken on the polished and thermally etched surface of the sintered body B. Bodies A and C exhibited similar microstructures. The information obtained with this conventional characterization tool is that there was no clear difference in the microstructure among samples A, B and C.

Fig. 9 shows photomicrographs taken in the transmission mode for thinned specimens of the sintered bodies. In contrast with the results of SEM observation

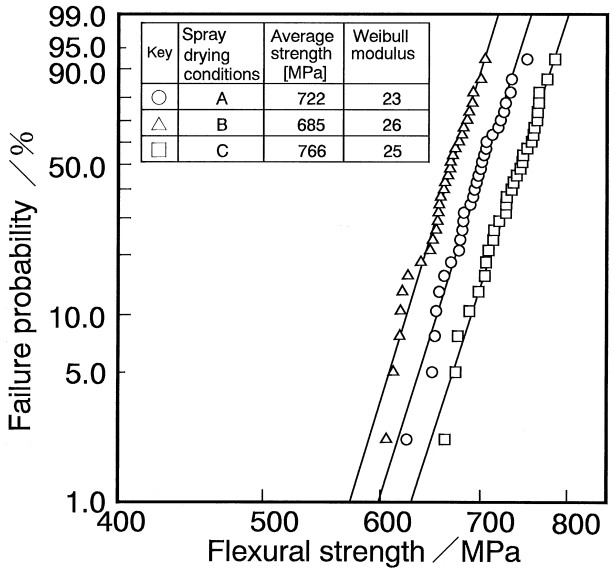

Fig. 7. Weibull distributions of the fracture strength for specimens.

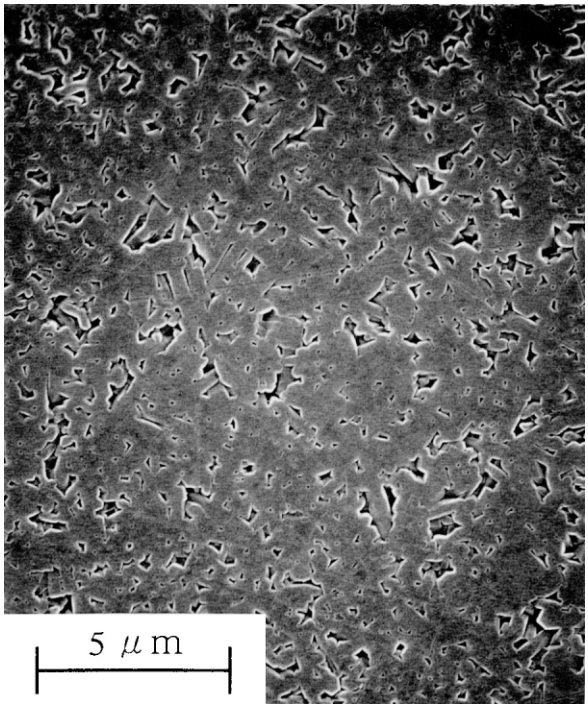

Fig. 8. Microstructure of ceramics specimen (B) by SEM.

(Fig. 8), heterogeneity was clearly noted in the internal microstructure as dark spots at the center and boundaries of granules. Comparison of the size distribution of dark spots reveals that the pore defect size is clearly smaller for sample C than for samples A and B, suggesting that there is correlation between the internal pore size distribution and the fracture strength as presented in Fig. 7. However, a difference of pore structure is not evident between samples A and B from the photographs.

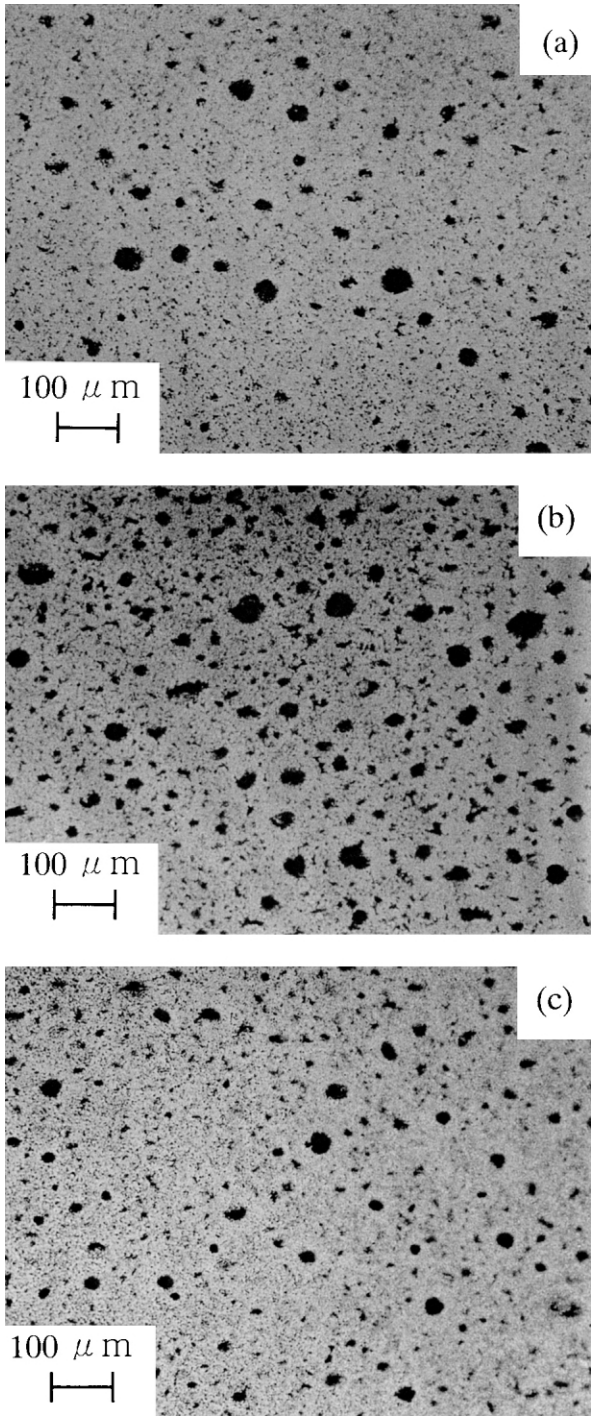

Fig. 9. Transmission optical micrographs of the thinned ceramics specimens. (a) A, (b) B, (c) C.

Fig. 10 shows the relation between the concentration and the size of large pores for all samples determined using the photomicrographs in the transmission mode. The pore concentration is defined as the number of pores per unit volume of specimen per unit size interval. For determining the pore concentration, the number of pores was counted using 5 μm, intervals, and plotted on the figure as the intermediate value in the interval. Pores

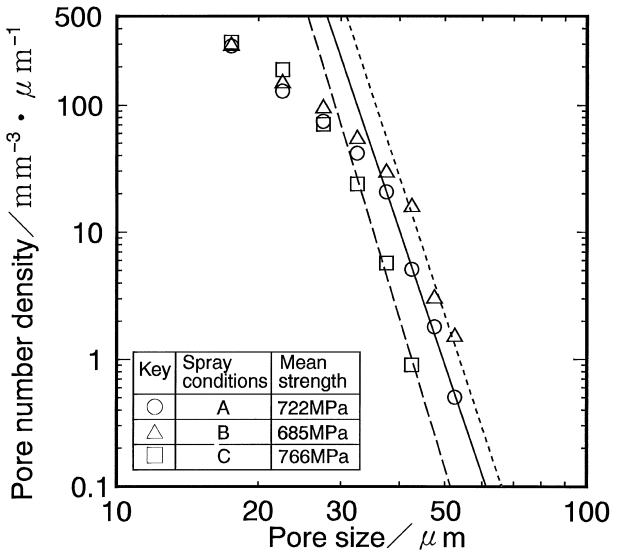

Fig. 10. Relation between pore number density and the pore size for the samples.

were assumed to have a spherical shape, and their size was represented by the equivalent diameter. The effective volume of specimens subjected for the examination was about 2.5 mm^3 for all samples, and the size was measured for about 2000 pores in each specimen. As presented in Fig. 10, the curves appear to be divided into two regions. In the region of small pore defects with less than about 30 μm, the pore density follows nearly the same line. On the other hand, the distribution curves show nearly parallel lines in the large pore region. The results indicate that internal pores become larger in the order of the sintered bodies C, A and B in agreement with the tendency of the fracture strength as shown in Fig. 7.

4. Discussion

The fracture strength of silicon nitride ceramics is strongly influenced by the pore defects introduced in the material during processing. As shown in Figs. 7 and 10, variation of the fracture strength can be explained by the pore size distribution found in the specimens. According to fracture mechanics, the strength σ, can be related to the size of the fracture origin, c, by the equation

$$K_{IC} = \sigma Y c^{1/2} \quad (1)$$

where K_{IC} is the fracture toughness and Y is a shape factor. As shown, the strength is inversely proportional to the one-half power of the size of the fracture origin for a given fracture toughness. Here we focus on the case where one defect can be found in the effective volume (one defect/2.5 mm^3). Because the number of pores is counted for a 5μm interval, the pore number density for this case becomes nearly 0.1 mm^{-3} μm^{-1} (1/2.5 mm^3/5 μm = 0.08). Focused on the pore sizes for all specimens at that concentration, Fig. 10 shows that the ratio of pore defect size becomes 1.27:1.17:1 for each specimen B:A:C provided that the curves can be extrapolated to the region of such large defects. Substituting the ratios of pore defect size and the fracture toughness in Table 2 to the above equation (1) gives that the size difference should correspond to 1.13 and 1.04 times higher strength for samples C and A, respectively, than for B, provided that the shape factor is assumed to be the same. The average strength (Fig. 7) for the samples C (766 MPa) and A (722 MPa) is 1.12 and 1.05 times larger than for the sample B (685 MPa). As reported for alumina,[5,6] the results demonstrate the relevance of the internal pore structure to the mechanical properties of the sintered material.

The results show that the fracture origin of the present sintered silicon nitride was the large pore defects developed from the potential flaws, large voids, in the green compacts during the subsequent densification and microstructure development. Here, the apparent high concentration of pores in Fig. 9 can be ascribed to the unique observation method of the present study, in which pores located at various depths in the specimens are observed simultaneously. The high concentration of pores with uniform distribution explains the high Weibull modulus of the present specimens.

As shown in Figs. 6 and 9, large voids preserved in and between granules during compaction should be the major source for the development of the pore defects in these sintered bodies. It has been known that the development of pores during sintering can be explained by a thermodynamic approach.[15,16] This recognizes that pores larger than a critical size are thermodynamically stable and can persist or grow during densification. In the case of silicon nitride densified by liquid phase sintering, however, non-uniform powder packing in granular compacted green bodies can contribute to making large pores grow by differential sintering with the re-distribution of the liquid phase from large pores to the near-by densifying region.[13] The present results show again the existence of local "large heterogeneities", large voids with non-uniform powder packing at and around them, in green compacts made by the granular compaction route.

The difference of the size distribution of pore defects among the sintered bodies A, B and C should be related to that of the potential flaws in the green compacts, if the densification and microstructure development are assumed to proceed in the same manner for all samples. It can, therefore, be considered that the size of potential flaws would be the largest for green compact B whereas the smallest for C.

Formation of potential flaws in green compacts can be ascribed to the non-uniform packing of powder particles

caused by the incomplete collapse of dimples in granules (Fig. 3) and of interstices between granules. The size and distribution of potential flaws should thus depend on the mechanical properties and the resultant compaction behavior of granules. The difference of fracture strength between the samples A and B, that are made from the granules with nearly the same size distribution, can be explained by the different deformation and/or fracture behavior of granules during compaction. As already described, the critical stress was the highest for granules B, 0.99 MPa, whereas the lowest for granules A, 0.75 MPa. This shows that granules B requires the highest compressive load for initiating the deformation at the contact points, because the critical stress is defined as the yield pressure at which granule rearrangement is essentially complete and granule deformation and/or fracture begins.[17] On the other hand, granules A have the lowest critical stress and, therefore, compaction of granules A should be more efficient for the reduction of coarse interstices in and between granules by the ease of deformation and fracture of them.

For sample C, another explanation is needed because granules C have larger size than granules A and B, and the critical stress of the granule bed is higher than that of granules A. Bisides, the gradients in the higher compressive stress (Fig. 4) cannot explain the difference for these three types of granules. The characteristics of granules C suggests that they would be detrimental for the reduction of the size of potential flaws in the green compacts, at least when compared with granules A. It is thus interesting that the sintered body C exhibited the highest fracture strength with the smallest pore defect size despite the detrimental characteristics of the granules for effective compaction.

Reduction of the defect size in sample C can be attributed to the different deformation and/or fracture behavior in granules C. Higher critical stress of granules C than A suggests that the granules should be less deformable during the initial stage of compression. A possible explanation for the reduction in size of the potential flaws in green compact C is the different fracture mechanism of granules C after deformation with increasing compaction pressure. Generally, granules slide past each other and are rearranged until the load reaches p_c, where the contact points deform plastically with increasing the consolidation stress. Finally, the granules are fractured when the stress exceeds the breakage value.[14] In the case of alumina, the authors have reported that the size of potential flaws can be reduced even when the granules with a high yield stress are used, provided that the granules fracture into many small fragments under a high applied pressure.[18] In this case, fragmentation of the granules to small pieces was considered to fill efficiently the void spaces in and between the granules and, as a result, to reduce the size of flaws. The same explanation may be possible in the present case, although the reason of allowing granules C to have such the unique characteristics is still unclear. Further examination thus should be needed on the fracture behavior of a single granule and the effect of it on the compaction of the granule bed in order to explain the reason for the different fracture behavior for granules C.

5. Conclusion

Differences in the fracture strength of sintered silicon nitride made from the granular compaction route could be explained quantitatively by the difference in the size distribution of pore defects in the sintered bodies as determined by direct observation techniques. Potential flaws in green compacts, that were introduced by the non-uniform packing of powder particles resulted from the incomplete collapse of dimples in granules and of interstices between granules. They form large pore defects during sintering. Formation of the potential flaws during compaction depended on the mechanical properties and the resultant compaction behavior of the granules.

References

1. Lange, F. F., Powder processing science and technology for increased reliability. *J. Am. Ceram. Soc.*, 1989, **72**, 3–15.
2. Iwamoto, Y., Nomura, N., Sugiura, I., Tsubaki, J., Takahashi, H., Ishikawa, K., Shinohara, N., Okumiya, M., Yamada, T., Kamiya, H. and Uematsu, K., Microstructure evolution and mechanical strength of silicon nitride ceramics. *J. Mat. Res.*, 1994, **9**, 1208–1213.
3. Takahashi, H., Shinohara, N., Uematsu, K. and Tsubaki, J., Influence of granule character and compaction on the mechanical properties of sintered silicon nitride. *J. Am. Ceram. Soc.*, 1996, **79**, 843–848.
4. Shinohara, N., Okumiya, M., Hotta, T., Nakahira, K., Naito, M. and Uematsu, K., Effect of seasons on density, strength of alumina. *Am. Ceram. Soc. Bull.*, 1999, **78**, 81–84.
5. Hotta, T., Nakahira, K., Naito, M., Shinohara, N., Okumiya, M. and Uematsu, K., Origin of strength change in ceramics associated with the alteration of spray dryer. *J. Mater. Res.*, 1999, **14**, 2974–2979.
6. Shinohara, N., Okumiya, M., Hotta, T., Nakahira, K., Naito, M. and Uematsu, K., Seasonal variation of microstructure and sintered strength of Day-pressed alumina. *J. Am. Ceram. Soc.*, 1999, **82**, 3441–3446.
7. Naito, M., Hotta, T., Hayakawa, O., Shinohara, N. and Uematsu, K., Ball milling conditions of a very small amounts of large particles in silicon nitride powder. *J. Ceram. Soc. Japan*, 1998, **106**, 811–814.
8. Uematsu, K., Kim, J.-Y., Kato, Z., Uchida, N. and Saito, K., Direct observation method for internal structure of ceramic green body- alumina green body as an example. *J. Ceram. Soc. Japan*, 1990, **98**, 515–516.
9. Uematsu, K., Kim, J.-Y., Miyashita, M., Uchida, N. and Saito, K., Direct observation of internal structure in spray-dried alumina granules. *J. Am. Ceram. Soc.*, 1990, **73**, 2555–2557.
10. Uematsu, K., Miyashita, M., Kim, J.-Y., Kato, Z. and Uchida, N., Effect of forming pressure on the internal structure of

alumina green bodies examined with immersion liquid technique. *J. Am. Ceram. Soc.*, 1991, **74**, 2170–2174.
11. Uematsu, K., Tanaka, T., Zhang, Y. and Uchida, N., Liquid immersion–polarized light microscopy as a powerful tool in the research of ceramic processing. *J. Ceram. Soc. Japan*, 1993, **101**, 1400–1403.
12. Uematsu, K., Immersion microscopy for detailed characterization of defects in ceramic powders and green bodies. *Powder Technology*, 1996, **88**, 291–298.
13. Shinohara, N., Takahashi, H., Ohsaka, S., Hotta, T., Naito, M. and Uematsu, K., Comparative study of injection molding and powder compaction methods for silicon nitride ceramics. *J. Am. Ceram. Soc.*, submitted for publication.
14. Naito, M., Nakahira, K., Hotta, T., Ito, A., Yokoyama, T. and Kamiya, H., Microscopic analysis on the consolidation process of granule beds. *Powder Technology*, 1998, **95**, 214–219.
15. Kingery, W. D. and Francois, B., The sintering of crystalline oxides, I. Interactions between grain boundaries and pores. In *Sintering and Related Phenomena*, ed. G. C. Kuczynski, N. A. Gibbon and G. N. Gibbon. Gordon and Breach, New York, 1967, pp. 471–498.
16. Kellett, B. J. and Lange, F. F., Thermodynamics of densification: I, sintering of simple particle arrays, equilibrium configurations, pore stability, and shrinkage. *J. Am. Ceram. Soc.*, 1989, **72**, 725–734.
17. Messing, G. L., Markoff, C. J. and McCoy, L. G., Characterization of ceramic powder compaction. *Am. Ceram. Soc. Bull.*, 1982, **61**, 857–860.
18. Shinohara, N., Okumiya, M., Hotta, T., Nakahira, K., Naito, M. and Uematsu, K., Variation of the microstructure and fracture strength of cold isostatically pressed alumina ceramics with the alteration of dewaxing procedures. *J. Eur. Ceram. Soc.,* 2000, **20**, 843–849.
19. Naito, M., Hotta, T., Hayakawa, O., Shinohara, N., Okumiya, M. and Uematsu, K., New characterization techniques to control the manufactureing process of fine ceramics. In *Advances in Process Measurements for Ceramic Industry*, ed. A. Jillavenkatesa and G. Y. Onoda. American Ceramic Society, OH, 1999, pp. 87–105.